Solid phase drug-drug pharmaceutical co-crystal formed between pyrazinamide and diflunisal: Structural characterization based on terahertz/Raman spectroscopy combining with DFT calculation

Xiushan Wu [a,b], Yaguo Wang [c], Jiadan Xue [d], Jianjun Liu [c], Jianyuan Qin [c], Zhi Hong [c], Yong Du [c,*]

[a] School of Electrical Engineering, Zhejiang University of Water Resources and Electric Power, Hangzhou 310018, PR China
[b] College of Mechanical and Electrical Engineering, China Jiliang University, Hangzhou 310018, PR China
[c] Centre for THz Research, China Jiliang University, Hangzhou City, Zhejiang Province 310018, PR China
[d] Department of Chemistry, Zhejiang Sci-Tech University, Hangzhou City, Zhejiang Province 310018, PR China

ARTICLE INFO

ABSTRACT

Both pretty low solubility and high membrane permeability of diflunisal (DIF) would affect significantly its oral bioavailability as a typical non-steroidal anti-inflammatory substance. Meanwhile, pyrazinamide (PZA), known as one kind of important anti-tuberculosis drugs, has also several certain side effects. These deficiencies affect the large-scale clinical use of such drugs. Solid-state pharmaceutical co-crystallization is of contemporary interest since it offers an easy and efficient way to produce prospective materials with tunable improved properties. In the current work, a novel solid phase drug-drug co-crystal involving DIF and PZA with molar ratio 1:1 was prepared through the mechanical grinding approach, and vibrational spectroscopic techniques including terahertz time-domain spectroscopy (THz-TDS) and Raman spectroscopy were performed to identify DIF, PZA and their pharmaceutical drug-drug co-crystal. The absorption peaks observed in the THz spectra of the co-crystal were at 0.35, 0.65, 1.17, 1.31 and 1.42 THz respectively, which are obviously different from parent materials. Similarly, Raman spectra could also be used to characterize the difference shown between the co-crystal and parent compounds. Structures and vibrational patterns of three kinds of possible co-crystal theoretical forms (form I, II and III) between DIF and PZA have been simulated by performing density functional theory (DFT) calculations. Theoretical results and THz/Raman vibrational spectra of DIF-PZA co-crystal show that the DIF links to PZA via the carboxylic acid-pyridine hetero-synthon association establishing the theoretical form I, which is a much-higher degree of agreement with experimental results than those of other two co-crystal forms. These results provide us a unique method for characterizing the composition of co-crystal structures, and also provide a wealth of drug-drug co-crystal structural information for improving physicochemical properties and pharmacological activities of specific drugs at the molecular-level.

© 2018 Elsevier B.V. All rights reserved.

1. Introduction

In the pharmaceutical industry, the solubility of a specific drug directly affects its actual bioavailability in the human body. This is also an important reason that >70% of active pharmaceutical ingredients (APIs) could not enter the ultimate market because of their pretty poor water solubility [1–3]. Modifications of various solid-state forms by changing the underlying crystalline structures of given APIs are becoming a feasible way to improve their corresponding physicochemical properties [4,5], namely amorphous forms, polymorphs, hydrates/solvates, salts and co-crystals [6,7]. In particular, research on emerging solid-state co-crystallization has made tremendous progress over the past few decades, because it provides a reliable and also practical methodology to improve the pharmaceutical properties of APIs without making and/or breaking any covalent bonds within them, so that the corresponding bioavailability of co-crystals would be enhanced significantly comparing with that shown in either of the starting API species [8,9]. Typically, the co-crystal represents a unique solid-state form that is combined by non-covalent interactions between one of specific API component and another generally recognized as one kind of safe (GRAS) co-crystal co-formers (CCFs) [10,11]. Among them, multi-API (API-API, or also known as drug-drug) co-crystals are potential solid-state forms for improving the problem of drug fixed combinations [12,13]. In addition, multi-API co-crystals could improve or even enhance specific physicochemical and biopharmaceutical properties of

* Corresponding author.
  E-mail address: yongdu@cjlu.edu.cn (Y. Du).

API drugs [14,15], so that finally improve long-term drug compliance in patients with a large amount of drug treatment, reducing the risk of multiple medication on the body [13,16].

The present work involves the study of solid phase co-crystal formation between two APIs (diflunisal and pyrazinamide). Diflunsial (abbreviated as DIF), being classified as one of class II drugs in the biopharmaceutics classification system (BCS) with molecular structure as shown in Fig. 1a (left), is an important di-fluorphenyl derivative of salicylic acid [17]. As one of typically used nonsteroidal anti-inflammatory drugs (NSAIDs), DIF shows pretty low solubility and also high membrane permeability which would affect significantly its corresponding oral bioavailability of human body [18], so that DIF has

shown comparatively less clinical application binding to DNA than that of aspirin [19]. Pyrazinamide (abbreviated as PZA), as one of typical first-line anti-tuberculosis (anti-TB) drugs with molecular structure as shown in Fig. 1a (right), belongs to one of effective TB chemotherapy drugs recommended by the World Health Organization (WHO) [20,21]. However, in the previous report, as many as 40% of patients would appear side effects such as gastrointestinal disturbances, headache and systemic poly-articular pain after taking PZA drug for a long time, and they needed to take aspirin or other NSAIDs to relieve such pains [22]. Therefore, it is envisaged that the drug-drug co-crystallization of PZA-DIF could improve the solubility of DIF while reducing the damage of PZA to the human body. Such multi-API or
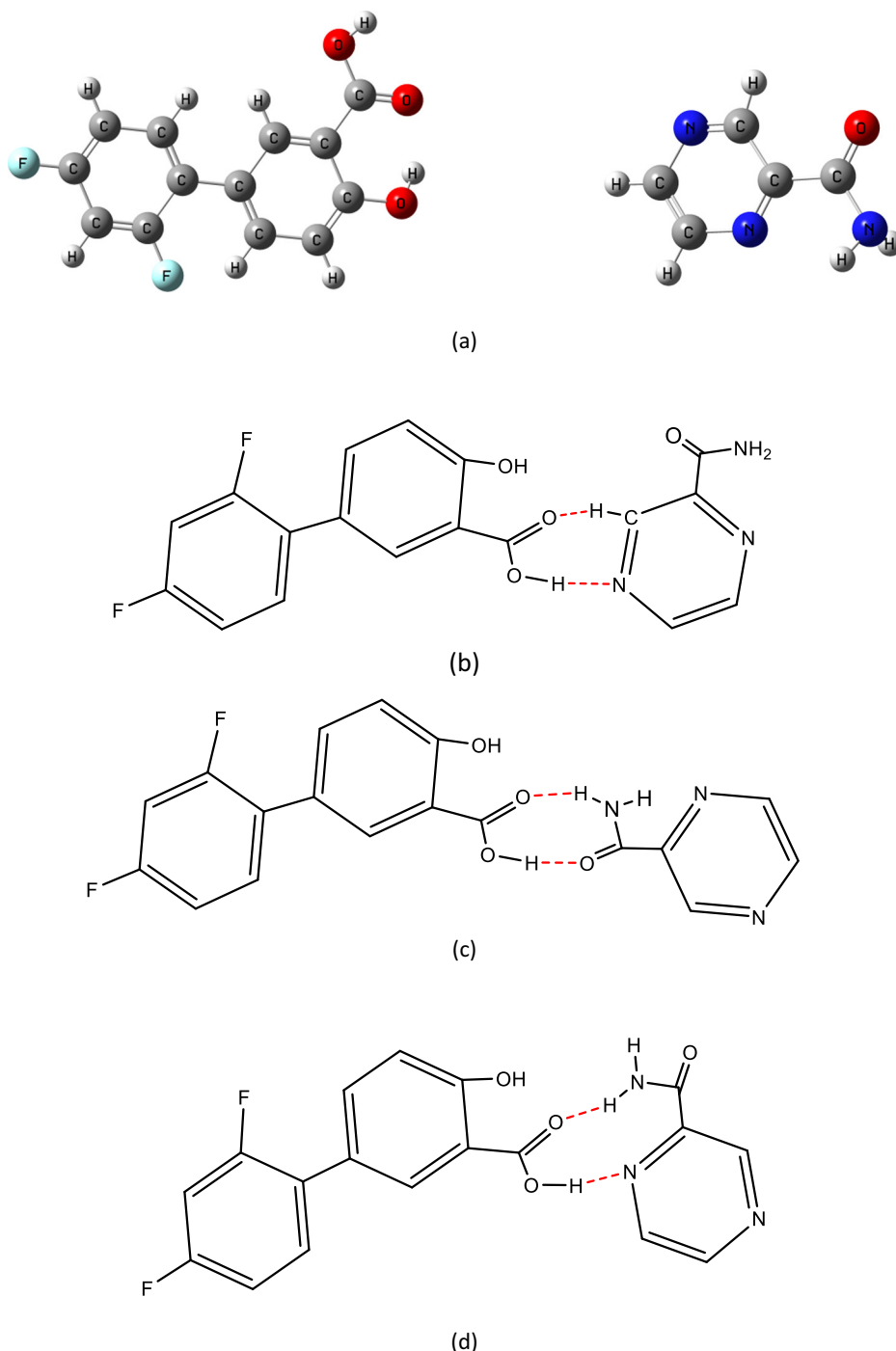

(a)

(b)

(c)

(d)

Fig. 1. Molecular structures of DIF, PZA (a), the theoretical PZA-DIF co-crystal form I (b), form II (c) and form III (d).

drug-drug structural modifications have been good explorations and alternatives for developing such combined-using drugs in the pharmaceutical research filed.

In previous literatures, based on the molecular attributes presenting in the molecules of DIF and PZA, a few number of solid phase co-crystals between these two APIs with various co-crystal formers (CCFs) have been reported [23–27], which can be found with 2:1 DIF-nicotinamide/isonicotinamide [23], 1:1 DIF-theophylline [24], 1:1 PZA-3-hydroxybenzoic acid [27], 1:1 PZA-p-toluenesulfonic acid/ferulic acid [26]. Also, the 1:1 PZA-DIF drug-drug co-crystal have been reported by Évora et al. [25]. They successfully prepared the co-crystal between DIF and PZA under grinding condition, and analyzed its corresponding structure using X-ray powder diffraction (PXRD), infrared spectroscopy (IR), polarized light thermal microscopy (PLTM), and differential scanning calorimetry (DSC), afterwards they found that the pharmacological effect of co-crystal between DIF and PZA could be almost compatible with those of two parent drugs, meanwhile the aqueous solubility of DIF was enhanced efficiently due to such co-crystallization [25]. Although Évora et al. [25] gave a partial introduction to the structure of DIF-PZA drug-drug co-crystal based on PXRD results, THz and Raman spectroscopic studies about such compound system at the molecular level have never been mentioned. In order to get a deeper understanding of the structures and specific hydrogen bonding patterns of co-crystal between DIF and PZA due to both intra-molecular and inter-molecular interactions, it is necessary to obtain such information based on vibrational spectroscopic techniques.

In the past decades, both emerging THz and normal Raman spectroscopy have been applied to the investigation into molecular structural information of specific solid-state compounds. THz spectroscopy is suitable for interrogating collective-molecular motions and detecting an increased number of vibrational modes shown in low-frequency region [28]. It is one of powerful tools for detecting vibrational modes, including from phonon, rotational and vibrational transitions [29], and is sensitive to both inter-molecular and intra-molecular interactions shown within specific crystalline materials [30–32]. Meanwhile, laser Raman spectroscopy, based on light scattering effect dependent on the vibrational normal coordinates due to the transition polarizability changes [32], is totally complementary to infrared and THz vibrational spectroscopy and allows for a complete description in fundamental vibrational motions and also structural changes shown within various solid-state crystalline polymorphs and co-crystals [33,34].

In this present work, in addition to using Raman/THz vibrational spectroscopy to characterize the vibrational modes of DIF-PZA solid phase drug-drug co-crystal and starting parent materials, the density functional theory (DFT), as a very useful method that could predict the intra-molecular and inter-molecular vibrational motions giving rise to the observed vibrational spectra [35,36], is also employed to enable the unambiguous assignment of each experimental spectra features. Both optimized geometries and vibrational mode assignments of different kinds of possible theoretical forms shown within the DIF-PZA drug-drug co-crystal have been proposed and also investigated regarding as various intra-molecular and inter-molecular interactions between DIF and PZA molecules.

2. Experiments and theoretical methods

2.1. Chemicals and sample preparation

Anhydrous solid-state DIF (purity 99%) was acquired by J&K Chemical Company (Shanghai, China). The sample PZA (purity 99%) was purchased from Sigma-Aldrich Company (Shanghai, China). All compounds were used as received without additional purification.

The DIF-PZA drug-drug co-crystal was obtained by liquid assisted grinding method, which is one of commonly used methods in the field of co-crystal preparation and analysis. At room temperature, the mixture of molar ratio 1:1 stoichiometry of DIF (0.01 mol, ~250 mg) and

PZA (0.01 mol, ~122 mg) was added in 25 ml stainless steel milling jars. Co-grinding the physical mixture was performed in an oscillatory ball mill (Mixer Mill MM400, with grinding-time lasting around 60 min and frequency at 15 Hz), and several drops of water (around 0.05 ml) was added to the mixture compounds before starting mechanical grinding in the planetary mill. In order to design a set of control experiment, another physical mixture was obtained by gently mixing two compounds above with a 1:1 equal-molar ratio in a glass vial by using a vortex mixer. Approximately 0.25 g DIF, PZA, physical mixture and the corresponding co-crystal were weighed and they were ground gently to achieve particles with the mean size of several micrometers in order to minimize the scattering effects from sample particles during THz spectral measurements. These samples were respectively prepared by using a hydraulic compression machine (HANDTAB-100, Ichihashi Seiki, Kyoto, Japan) with a diameter of about 13.00 mm and a thickness of around 1.60 mm. The pressure is continuously applied for 30 s at a constant pressure of around 4.0 MPa to obtain final pellets, and they are sealed in plastic bags in order to avoid probable deliquescence at room temperature before further THz spectral measurements. As for Raman spectral measurements, there is no need for further sample preparation.

2.2. THz/Raman apparatus and spectral measurements

The treated samples of DIF, PZA, their physical mixture and DIF-PZA drug-drug co-crystal were then placed in a time domain pulsed THz spectrometer (Zomega Co. Ltd., New York, NY, USA) to obtain their respective THz spectra. THz wave generation and detection were achieved through the non-linear optical effects of zinc telluride crystals due to photoconductive switch [37] and free-space electro-optic sampling [38], respectively, within a femtosecond laser system based on amplified Ti: Sapphire oscillator ultrafast laser pulse system with central wavelength 780 nm, pulse width 100 fs, and repetition frequency 75 MHz (Spectra Physics, Owen, CA, USA). The THz spectral experiments were performed entirely within a dry nitrogen chamber to avoid pretty strong absorption from water vapor.

Raman spectra of all samples were obtained using Fourier Transform Raman (FT-Raman) spectrometer (Thermo Nicolet Corporation, Madison, WI, USA) with diode pumped solid-state laser with wavelength 1064 nm as the near-IR source. Raman spectra were acquired over 256 scans at 2.0 cm^{-1} resolution with the laser operating power around 150 mW.

2.3. DFT theoretical calculations

The theoretical structures of DIF, PZA and their DIF-PZA drug-drug co-crystal were optimized at the DFT level using the B3LYP functional and 6-311++G (d, p) basis set implemented in the Gaussian'03 package [39,40]. Due to DIF and PZA owning multiple hydrogen-bonding sites, three kind of possible theoretical co-crystal forms have been suggested and calculated. DIF-PZA drug-drug co-crystal theoretical form I is a theoretical binary polymer formed by acid-pyridine hetero-synthon association under inter-molecular hydrogen bonding (shown in Fig. 1 (b)), while the theoretical co-crystal form II formed by carboxylic acid-amide association (shown in Fig. 1 (c)). As for the theoretical co-crystal form III, the hydrogen bonds are formed between carboxylic acid, and pyridine N and amide (shown in Fig. 1 (d)). Évora et al.[25] reported that the form I was the most reasonable structure of DIF-PZA drug-drug co-crystal by using PXRD in previous work, so as to better understand the hydrogen bond motifs and the role of hydrogen bonding in changing molecular structure of PZA and DIF, we further investigate the micro-molecular structures and vibrational modes of DIF-PZA drug-drug co-crystal by combining THz/Raman vibrational spectroscopy results with DFT calculation. Regarding as the simulated THz/Raman vibrational spectra, lorentzian line shapes were convolved into the

calculated modes using a full-width half-maximum (FWHM) value of 4.0 cm^{-1}.

3. Results and discussions

3.1. THz spectral characterization and analysis of DIF-PZA drug-drug co-crystal

Fig. 2 displays THz absorption features of DIF, PZA, their physical mixture and corresponding DIF-PZA drug-drug co-crystals prepared from liquid assisted grinding methods in the recorded spectral range of 0.2–1.6 THz. It could be clearly seen that both starting materials show significantly different absorption bands in the recorded frequency range. The absorption bands of DIF centered at 0.46 and 0.92 THz, PZA has two broad bands at 0.51, 0.74 THz and a high-intensity band at 1.48 THz respectively, in which all bands are consistent with the previously reported result from Wang Q. Q. et al. [27]. Meanwhile, the absorption bands of physical mixture centered at 0.50, 0.74, 0.92 and 1.55 THz, namely just the simple linear-superposition of both involved starting reactants (DIF and PZA). The spectrum of co-crystals obtained from liquid assisted grinding methods (as shown in Fig. 3d) present several characteristic bands at 0.35, 0.65, 1.17, 1.32 and 1.42 THz respectively those are not observed in the spectrum of their physical mixture. It is well known that the formation of co-crystallization would be induced by non-covalent bond interactions between multicomponent molecules such as hydrogen bonding, nonionic, etc. [41]. And, it had also been reported that THz spectroscopy could sensitively detect the low-frequency vibrational motion of molecular lattices from previous studies [34,42,43]. So, experimental THz results indicate that the involved starting reactants, DIF and PZA, form the co-crystal structure successfully through non-covalent bond interactions, especially the driving forces of strong inter-molecular hydrogen bonding. Meanwhile in the physical mixture such hydrogen bond and/or other non-covalent interactions are never involved during the simple physical mixing process between DIF and PZA.

Comparison between experimental THz spectral result and DFT theoretical spectra of three kind of possible theoretical co-crystal forms between DIF and PZA is shown in Fig. 3. In the THz spectrum, the molecular vibration effects in the co-crystal cause the generation and disappearance of characteristic peaks, and these vibration effects are directly related to different vibration modes, such as stretching, bending, torsion, scissor and deformation vibrations. As shown in Fig. 3, the form II and form III have two characteristic bands respectively, which
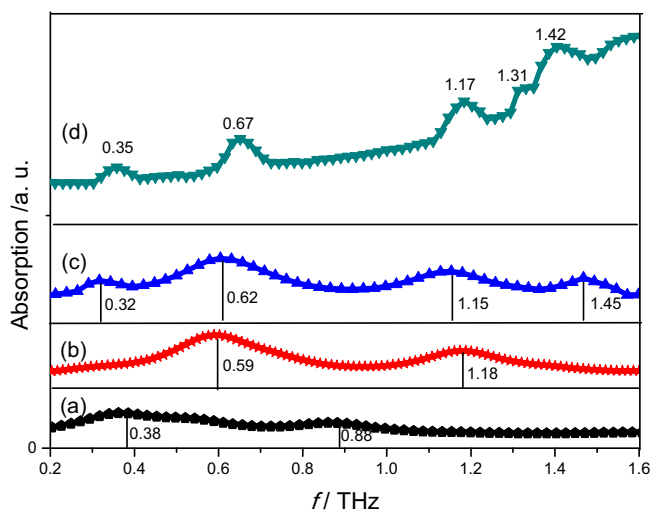

Fig. 3. Comparison of THz absorption spectra of PZA-DIF co-crystal between theoretical (form III (a), form II (b) and form I (c)) results and experimental result (d).

differ significantly from bands shown in the experimental THz spectrum of DIF-PZA drug-drug co-crystal. But the form I have four characteristic bands at positions of 0.32, 0.65, 1.15, 1.45 THz, which are much highly closer to the experimental spectral results than those of other two forms (form II and form III). It is not difficult to find that the characteristic bands of theoretical form I has a red-shift and experiment result have no corresponding characteristic band comparing with theoretically calculated spectral results at 1.31 THz. The reason for the above inconsistency between theoretical and experimental results may be that the THz experimental spectrum is obtained at room temperature but theoretical simulation is performed at an absolute temperature of absolute zero degree [44]. Moreover, different computing functional and basis sets may also cause some inconsistency between theory and experiment. According to the above analysis, it could be demonstrated that the structure being the theoretical co-crystal form I is much more suitable than other two forms upon drug-drug co-crystallization between DIF and PZA. This induction is also consistent with the result reported by the Évora et al. [25].

Fig. 4 shows different vibrational modes distribution about the absorption bands of theoretical co-crystal form I. All of these vibrational modes distribution is described in Table 1. The vibrational modes distribution at 0.32 THz caused by the torsional vibration of DIF and PZA (as shown in Fig. 4(a)), which is corresponding to experimental spectrum at 0.35 THz. The O24=C21-O25-H35 of DIF out plane bending vibration, and PZA torsional vibration make contribution to the mode distribution at 0.82 THz (as shown in Fig. 4(b)), and it is consistent with the experimental spectra feature at 0.87 THz. The characteristic band at 1.15 THz corresponds to the experimental spectrum at 1.17 THz, which is caused by in plane bending and O24=C21-O25-H35 out plane bending vibration with DIF molecular and PZA molecular torsion vibration. The characteristic band at 1.45 THz corresponds to the experimental spectrum at 1.42 THz (as shown in Fig. 4 (c)), which is due to DIF molecular out plane bending vibration, O24=C21-O25-H35 of DIF in plane bending vibration and PZA in plane bending vibration. As for the THz spectrum, its absorption mechanism is mainly due to the excitation of low frequency vibrational motions in crystalline samples, such as optical rotation and translation, which could be used to sensitively detect hydrogen bonding effect between various model molecules [34,43,45]. So, by comparing experimental THz spectrum result with DFT simulation, the hydrogen bonding effect between DIF and PZA plays a key role in changing the individual molecular structure of such two parent
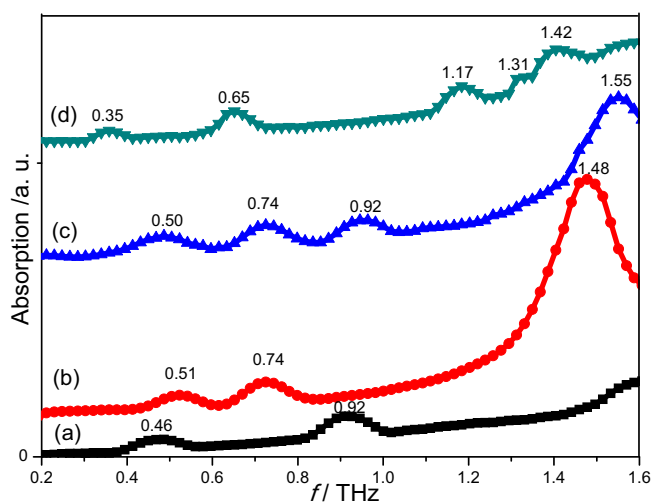

Fig. 2. The THz spectra of DIF (a), PZA (b), physical mixture (c) and PZA-DIF co-crystal (d) in 0.2–1.6 THz spectral region.
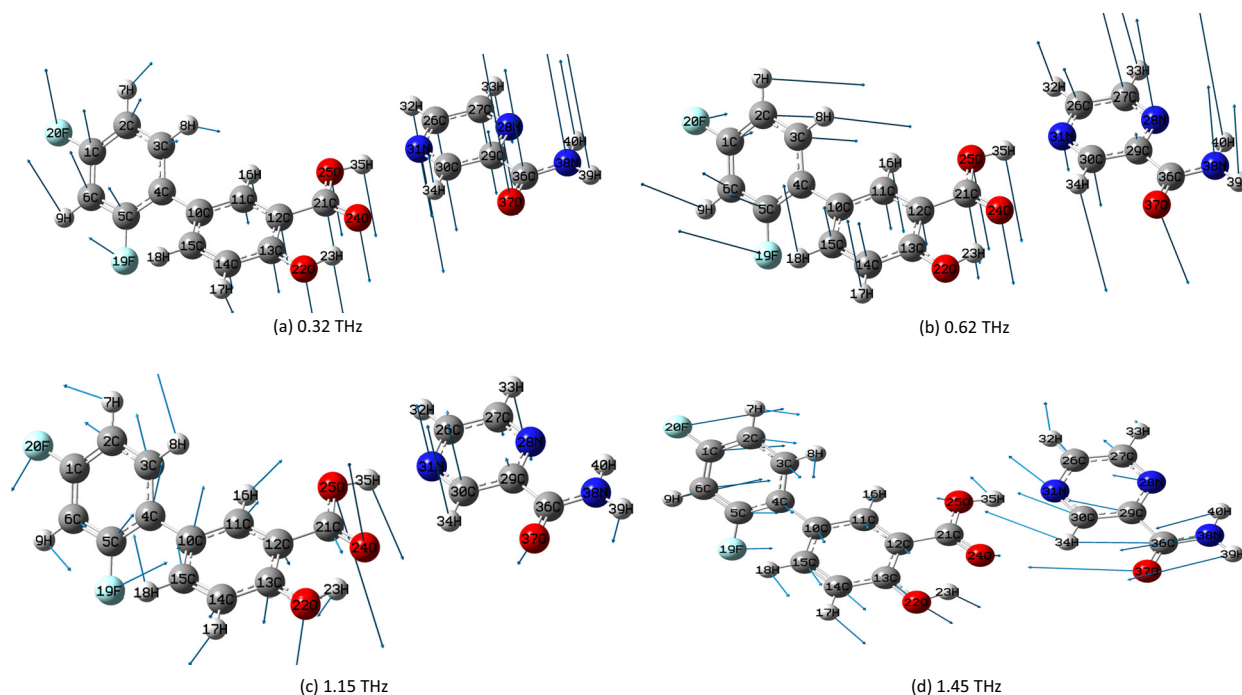
Fig. 4. Vibrational mode description of co-crystal formed between DIF and PZA at the position of 0.32 (a), 0.62 (b), 1.15 (c) and 1.45 (d) THz.

materials upon their drug-drug co-crystal formation, which makes the vibrational modes of the PZA-DIF co-crystal different from those of the starting compounds.

3.2. Raman spectral characterization and analysis of DIF-PZA drug-drug co-crystal

Fig. 5 displays the experimental Raman vibrational spectra of DIF, PZA, physical mixture and their co-crystal. As seen from this diagram, there are several new characteristic peaks and band shifts observed in the frequency range of 200–1800 cm^{-1}. Here, the Raman spectrum of DIF is agreement with the polymorph I reported by the previous Pallipurath's work [46]. As for the Raman spectrum of DIF-PZA drug-drug co-crystal, several unique characteristic peaks at 244, 1185, 1370, 1406 and 1750 cm^{-1} respectively are marked with blue rectangular shadows, while such features could not be found in that of physical mixture and also starting materials. Similarly, in the spectrum of physical mixture, there is a weak peak at 807 cm^{-1}, which is mainly contributed by DIF but disappears within that of DIF-PZA drug-drug co-crystal. In addition, the position at 458 and 1620 cm^{-1} in the spectrum of the physical mixture, arising from PZA, are red-shifted to be at 449 and 1612 cm^{-1} along with the formation of DIF-PZA drug-drug co-crystal respectively. The differences in these Raman spectra demonstrate that the drug-drug co-crystal between DIF and PZA has been successfully formed, whose crystalline phase and structure are totally different from those of the raw parent materials.

Fig. 6 shows the Raman spectral comparison between experimental and theoretical (just shown with form I due to the consistency between them) results for DIF-PZA drug-drug co-crystal. And the vibrational mode assignments for Raman characteristic peaks of the co-crystal between DIF and PZA are completely portrayed in Table 2. It could be seen that the theoretical simulated spectrum is pretty consistent with the experimental result. The characteristic peak at 244 cm^{-1} in the

Table 1
Vibrational mode assignment of the DIF-PZA drug-drug co-crystal shown in the THz spectrum.

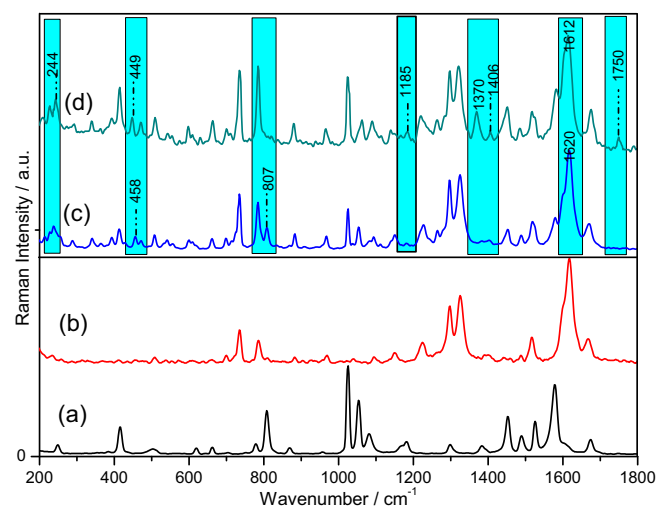| Experimental result f / THz	Theoretical calculation f / THz	Mode assignment
0.35	0.32	DIF molecular torsional vibration; PZA molecular torsion vibration
0.87	0.82	PZA molecular torsional vibration; O24 = C21-O25-H35 out plane bending vibration
1.17	1.15	DIF in plane bending; O24 = C21-O25-H35 out of plane bending vibration; PZA molecular torsional vibration
1.42	1.45	PZA in plane bending vibration; DIF molecular out of plane bending vibration; O24 = C21-O25-H35 in plane bending vibration

Fig. 5. Experimental Raman spectra of DIF (a), PZA (b), physical mixture (c), and co-crystal (d).
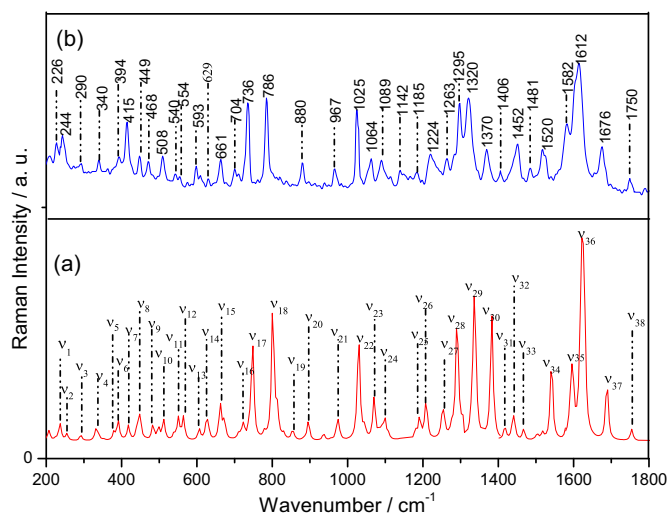
Fig. 6. Comparison of Raman spectra of theoretical form I (a) with experimental result (b) about co-crystal formed between DIF and PZA.

experimental result, arises from out-of plane bending vibration $\omega(R1)$ and torsional vibration $\tau(C1\text{-}F20)$ in DIF (R1: six-membered benzene ring) and such structure could be seen in Fig. 7. The feature at position of 1185 cm^{-1}, is caused by out-of-plane bending vibration $\omega(O25\text{-}$

H35) in DIF and in-plane bending vibration $\rho(H39\text{-}N38\text{-}H40)$, scissoring vibration $\delta(H32\text{-}C26\text{-}C27\text{-}H33)$ in PZA. Meanwhile, the band at 1370 cm^{-1}, is generated from in-plane bending vibration $\rho(O25\text{-}H35)$, out-of-plane bending vibration $\omega(O24{=}C21\text{-}O25)$ in DIF, and deformation vibration Def(R3), out-of-plane bending vibration $\omega(C26\text{-}H32)$ in PZA. While the peak at the position of 1406 cm^{-1} in experimental spectra is caused by in-plane bending vibration $\rho(O22\text{-}H23, C11\text{-}H16, C15\text{-}H18)$ and out-of-plane bending vibration $\omega(C21\text{-}O25\text{-}H35)$ within DIF, out-of-plane bending vibration $\omega(C30\text{-}H34)$ in PZA. Another weak new peak at position 1750 cm^{-1} would appear in the spectrum of DIF-PZA drug-drug co-crystal, arising from stretching vibration $\theta(C21{=}O24, C21\text{-}O25)$ in DIF, and stretching vibration $\theta(C36\text{-}N38, C36{=}O37)$, out-of-plane bending vibration $\omega(C29\text{-}C36)$ in PZA. Similarly, the characteristic band at the position of 1612 cm^{-1}, which had shown some red-shift relative to physical mixture, is caused by stretching vibration $\theta(C21{=}O24, C21\text{-}O25, C11\text{-}C12)$, in-plane bending vibration $\rho(O25\text{-}H35)$, out-of-plane bending vibration $\omega(C13{=}O22\text{-}H23)$ and deformation vibration Def(R2) within DIF molecular. From the vibrational modes assignment of the above characteristic peaks, it could be inferred that the hydrogen bonding formation in carboxylic acid-pyridine hetero-synthon association between DIF and PZA plays an important role in its corresponding co-crystallization process. These Raman spectral results once again confirmed that the complexation of the DIF-PZA drug-drug co-crystal, because of the effect of hydrogen bonding associations, is the key point to such co-crystal formation, rather than a simple physical mixture of the two starting parent reactants (DIF and PZA).

Table 2
Vibrational mode assignment for characteristic bands of the DIF-PZA drug-drug co-crystal between DIF and PZA shown in the Raman spectrum.

Mode	Theoretical wavenumber/cm^{-1}	Experimental wavenumber/cm^{-1}	Mode assignment
ν_1	232	226(vw)	$\rho(R3)$
ν_2	250	244(w)	$\omega(R1)\tau(C1\text{-}F20)$
ν_3	293	290(vw)	$\omega(O24{=}C21\text{-}O25\text{-}H35, H40\text{-}N38\text{-}H39)$
ν_4	336	340(w)	$\omega(O24{=}C21\text{-}O25\text{-}H35, R1)$
ν_5	381	394(vw)	$\tau(R2)\omega(O24{=}C21\text{-}O25\text{-}H35, C13\text{-}O22\text{-}H23)$
ν_6	398	415(m)	$\omega(C21\text{-}O25\text{-}H35)\tau(R1)$
ν_7	422	449(w)	$\rho(R2, C13\text{-}O22\text{-}H23, O24\text{-}C21\text{-}O25\text{-}H35)$
ν_8	452	468(w)	$\tau(R3, C36\text{-}N38\text{-}H40)$
ν_9	483		$\omega(C36\text{-}O37)\rho(C30\text{-}H34, C27\text{-}H33)$
ν_{10}	512	508(w)	$\delta(H9\text{-}C6\text{-}C1\text{-}F20)$
ν_{11}	546	540(vw)	$\omega(C13\text{-}O20\text{-}H23)\text{Def}(R1)$
ν_{12}	560	554(vw)	$\tau(H18\text{-}C15\text{-}C14\text{-}H17)\omega(C13\text{-}O20\text{-}H23, F20\text{-}C1{=}C2\text{-}H7)$
ν_{13}	605	593(w)	$\omega(H7\text{-}C2\text{-}C3\text{-}H8, C14\text{-}H17)$
ν_{14}	629	629(vw)	$\omega(H8\text{-}C15\text{-}C14\text{-}H17, C6\text{-}H9)$
ν_{15}	663	661(m)	$\text{Def}(R3)\rho(H40\text{-}N38\text{-}H39)$
ν_{16}	718	704(vw)	$\tau(O24{=}C21\text{-}O25\text{-}H35)\omega(C14\text{-}H17)$
ν_{17}	748	736(s)	$\tau(H39\text{-}N38\text{-}H40, O25\text{-}H35)\omega(C11\text{-}H16)\text{Def}(R1)$
ν_{18}	798	786(s)	$\delta(O24{=}C21\text{-}O25\text{-}H35)\omega(C13\text{-}O22\text{-}H23, C30\text{-}H34,)$
ν_{19}	815		$\text{Def}(R3)\omega(O24{=}C21\text{-}O25\text{-}H35)\rho(H39\text{-}N38\text{-}H40)$
ν_{20}	895	880(m)	$\text{Def}(R2)\omega(O24{=}C21\text{-}O25\text{-}H35)\rho(C13\text{-}O22\text{-}H23)$
ν_{21}	974	967(m)	$\rho(C6\text{-}H9, C3\text{-}H8)\omega(F20\text{-}C1{=}C2\text{-}H7)$
ν_{22}	1031	1025(s)	$\rho(C30\text{-}H34, H39\text{-}N38\text{-}H40)\ \text{Def}(R3)$
ν_{23}	1072	1064(m)	$\rho(H17\text{-}C14\text{-}C15\text{-}H18, C11\text{-}H16, C6\text{-}H9)$
ν_{24}	1098	1089(m)	$\delta(H32\text{-}C26\text{-}C27\text{-}H33)\omega(C30\text{-}H34)$
ν_{25}	1188	1185(vw)	$\rho(H39\text{-}N38\text{-}H40)\delta(H32\text{-}C26\text{-}C27\text{-}H33)\omega(O25\text{-}H35)$
ν_{26}	1212	1224(m)	$\rho(C30\text{-}H34, C26\text{-}H32)\omega(C27\text{-}H33)$
ν_{27}	1252	1263(w)	$\tau(C21\text{-}O25\text{-}H25)\rho(C11\text{-}H16)\omega(C26\text{-}H32)$
ν_{28}	1291	1295(s)	$\rho(C30\text{-}H34, C27\text{-}H33)$
ν_{29}	1331	1320(s)	$\text{Def}(R1)\rho(C27\text{-}H33)\tau(O25\text{-}H35)\omega(C13\text{-}O22\text{-}H23)$
ν_{30}	1380	1370(s)	$\rho(O25\text{-}H35),\omega(O24{=}C21\text{-}O25, C26\text{-}H32),\text{Def}(R3)$
ν_{31}	1413	1406(vw)	$\rho(O22\text{-}H23, C11\text{-}H16, C15\text{-}H18)\omega(C21\text{-}O25\text{-}H35, C30\text{-}H34)$
ν_{32}	1456	1452(s)	$\omega(N31\text{-}C30\text{-}H34, C21\text{-}O25\text{-}H35)\rho(C26\text{-}H32)\delta(H39\text{-}N38\text{-}H40)$
ν_{33}	1475	1481(vw)	$\tau(O24{=}C21\text{-}O25\text{-}H35)\ \rho(C13\text{-}O22\text{-}H23, H32\text{-}C26{=}C27\text{-}H33)$
ν_{34}	1538	1520(m)	$\text{Def}(R1,R2),\rho(H17\text{-}C14\text{-}C15\text{-}H18, H7\text{-}C2\text{-}C3\text{-}H8)\omega(C13\text{-}O22\text{-}H23)$
ν_{35}	1592	1582(s)	$\theta(C21{=}O24, C11\text{-}C12)\ \omega(C13\text{-}O22\text{-}H23)\rho(O25\text{-}H35)$
ν_{36}	1620	1612(s)	$\theta(C21{=}O24, C21\text{-}O25, C11\text{-}C12)\rho(O25\text{-}H35)\omega(C13\text{-}O22\text{-}H23)\text{Def}(R2)$
ν_{37}	1691	1676(s)	$\theta(C21{=}O24\ \rho(C30\text{-}H34, O22\text{-}H23)\delta(C21\text{-}O25\text{-}H35)$
ν_{38}	1758	1750(w)	$\theta(C21{=}O24, C36\text{-}N38, C36{=}O37, C21\text{-}O25)\omega(C29\text{-}C36)$

vw—very weak, w—weak, m—medium, s—strong, θ—stretching vibration, ρ—in plane bending vibration, ω—out of plane bending vibration, τ—torsional vibration, δ—scissoring vibration, Def—Deformation.
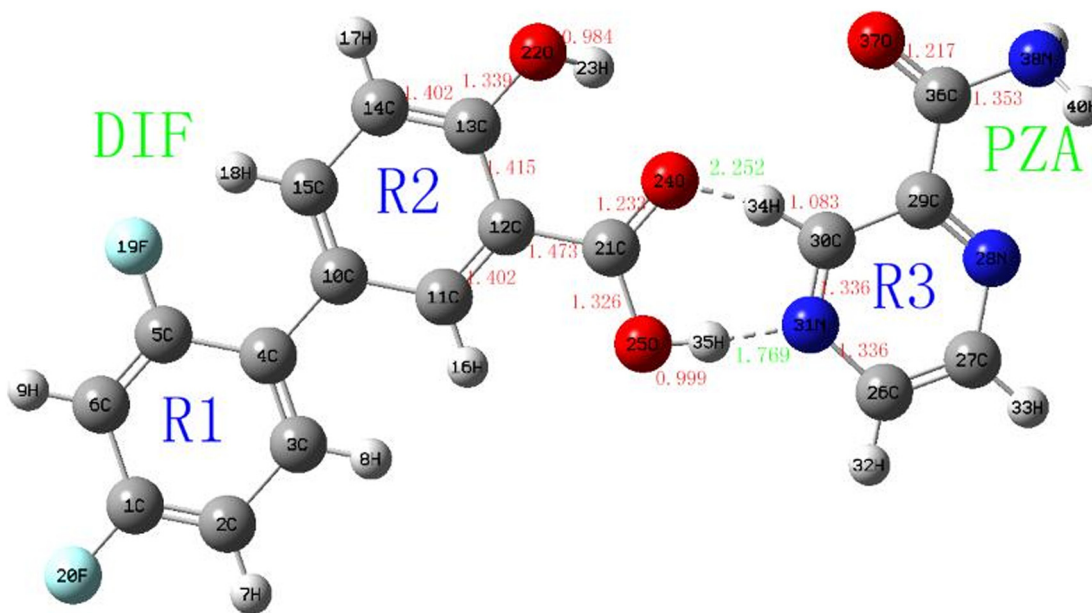
Fig. 7. Typical bond lengths (unit shown with Å) of co-crystal formed between DIF and PZA.

It is known to us, the micro-molecular structural information of co-crystal between DIF and PZA could be clearly characterized by the characteristic vibrational modes information based on both THz and Raman spectra. In order to gain a deeper insight into the structural information of DIF-PZA drug-drug co-crystal, the study of typical bond length changes upon co-crystallization and its relationship with characteristic vibrational bands have been carried out in this present work. Combining with the information of Fig. 7 and Table 3, a strong nonconventional carboxylic acid- pyridine C21=O24···H34, O25-H35···N31 inter-molecular hydrogen bond lengths are 2.252 Å and 1.769 Å, which are both belong to the category of typical hydrogen bond lengths respectively. Under the action of the above inter-molecular hydrogen bonds, some typical bond lengths have been changed during the co-crystallization process. Such as, the bond lengths of C21=O24, C21-O25 shown in DIF would be shortened from 1.287, 1.461 to 1.233, 1.326 Å respectively upon its drug-drug co-crystallization, which leads to the characteristic peak at 1750 cm^{-1}, also causes the blue-shifted of the corresponding co-crystal at position of 1620 cm^{-1} relative to the Raman spectrum of physical mixture at position of 1612 cm^{-1}. The bond length of N31=C30, C30-H34 in PZA are turned from original 1.238, 1.051 Å to 1.336, 1.083 Å, respectively (as shown in Fig. 7).

Other changes of typical bond lengths within co-crystal comparing with those of starting materials have been listed in detail in Table 3. The change in length of these chemical bonds may be related to characteristic peaks' shift, appearance and/or disappearance shown in the above normal Raman and emerging THz vibrational spectra upon pharmaceutical DIF-PZA drug-drug co-crystallization formation.

4. Conclusion

In the present work, we focus on the investigation of structures and vibrational modes of solid-state DIF-PZA pharmaceutical drug-drug co-crystal based on emerging THz and normal Raman spectroscopic techniques. Both vibrational spectra obtained in the measurement region provide finger-printing spectral information of co-crystal and starting materials. In order to deeply study the structural information due to intra-molecular and inter-molecular interactions between DIF and PZA molecules at molecular level contained in the co-crystal also infer the structural form it might have, the DFT calculation of three kinds of possible theoretical co-crystal forms between DIF and PZA were performed. As indicated by theoretical DFT calculation, the co-crystal formed by carboxylic acid-pyridine hetero-synthon (carboxylic•••pyridine) association under inter-molecular hydrogen bonding is most reasonable structure. It could be concluded that the interactions of inter-molecular hydrogen bonding shown in pharmaceutical co-crystallization could be well demonstrated by using THz and Raman vibrational spectroscopy. These results provide theoretical and experimental benchmarks for both structural and vibrational spectroscopic studies in the emerging pharmaceutical co-crystallization research and development fields.

Table 3
Change of typical chemical bond lengths between DIF, PZA and their drug-drug co-crystal.

Chemical bond	Bond length/Å		
	DIF	PZA	DIF-PZA co-crystal
C21=O24	1.287	–	1.233
C21-O25	1.467	–	1.326
O25-H35	0.958	–	0.999
C21-C12	1.540	–	1.473
C12-C13	1.540	–	1.415
C13-O22	1.430	–	1.339
O22-H23	0.960	–	0.984
C13-C14	1.355	–	1.402
N31=C30	–	1.238	1.366
C30-H34	–	1.051	1.083
C36-N38	–	1.353	1.470
C36=O37	–	1.217	1.258
C30-C29	–	1.530	1.397
N31-C26	–	1.336	1.461

CRediT authorship contribution statement

Xiushan Wu: Conceptualization, Data curation, Methodology, Software, Writing - review & editing. **Yaguo Wang:** Conceptualization, Data curation, Investigation. **Jiadan Xue:** Funding acquisition, Software, Validation, Writing - review & editing. **Jianjun Liu:** Methodology, Investigation. **Jianyuan Qin:** Visualization, Investigation. **Zhi Hong:** Funding acquisition, Methodology, Writing - review & editing. **Yong Du:** Funding

acquisition, Project administration, Writing - original draft, Writing - review & editing.

Declaration of competing interest

The authors declare that they have no known competing financial interests or personal relationships that could have appeared to influence the work reported in this paper.

References

[1] P.C. Vioglio, M.R. Chierotti, R. Gobetto, Pharmaceutical aspects of salt and corycrystal forms of APIs and characterization challenges, Adv. Drug Deliv. Rev. 117 (2017) 178–195.

[2] Z. Zhou, H.M. Chan, H.H.Y. Sung, H.H. Tong, Y. Zheng, Identification of new cocrystal systems with stoichiometric diversity of salicylic acid using thermal methods, Pharm. Res. 33 (2016) 1030–1039.

[3] H. Yamashita, C.C. Sun, Improving dissolution rate of carbamazepine-glutaric acid cocrystal through solubilization by excess conformer, Pharm. Res. 35 (2017) 651–663.

[4] C.B. Aakeröy, S. Forbes, J. Desper, Using cocrystals to systematically modulate aqueous solubility and melting behavior of an anticancer drug, J. Am. Chem. Soc. 131 (2009) 17048–17049.

[5] D. Walsh, D.R. Serrano, Z.A. Worku, B.A. Norris, A.M. Healy, Production of cocrystals in an excipient matrix by spray drying, Int. J. Pharm. 536 (2018) 467–477.

[6] R. Shaikh, R. Singh, G.M. Walker, D.M. Croker, Pharmaceutical cocrystal drug products: an outlook on product development, Trends Pharmacol. Sci. 39 (2018) 1033–1048.

[7] H.L. Sung, Y.L. Fan, K. Yeh, Y.F. Chen, L.J. Chen, A new hydrate form of diflunisal precipitated from a microemulsion system, Colloids Surf. B: Biointerfaces 109 (2013) 68–73.

[8] X. Ma, W. Yuan, S.E. Bell, S.L. James, Better understanding of mechanochemical reactions: Raman monitoring reveals surprisingly simple 'pseudo-fluid' model for a ball milling reaction, Chem. Commun. (Camb) 50 (2014) 1585–1587.

[9] X.F. Hu, T. Burgi, In situ ATR-FTIR investigation of photodegradation of 3,4-dihydroxybenzoic acid on TiO2, Catal. Lett. 146 (2016) 2215–2220.

[10] P. Vishweshwar, J.A. McMahon, J.A. Bis, M.J. Zaworotko, Pharmaceutical co-crystals, J. Pharm. Sci. 95 (2006) 499–516.

[11] U.S. Food and Drug Administration - Database of Select Committee on GRAS Substances (SCOGS) Reviews. http://www.accessdata.fda.gov/scripts/fcn/fcnNavigation.cfm?rpt=scogsListing (accessed 15/02/2011).

[12] S. Frantz, The trouble with making combination drugs, Nat. Rev. Drug Discov. 5 (2006) 881–882.

[13] F. Pan, M.E. Chernew, A.M. Fendrick, Impact of fixed-dose combination drugs on adherence to prescription medications, J. Gen. Intern. Med. 23 (2008) 611–624.

[14] N.J. Babu, A. Nangia, Solubility advantage of amorphous drugs and pharmaceutical cocrystals, Cryst. Growth Des. 11 (2011) 2662–2679.

[15] M. Rodrigues, B. Baptista, J.A. Lopes, M.C. Sarraguca, Pharmaceutical cocrystallization techniques. Advances and challenges, J. *Int. Pharm.* 547 (2018) 404–420.

[16] E. Vermeire, H. Hearnshaw, P. Van Royen, J. Denekens, Patient adherence to treatment: three decades of research. A comprehensive review, J. Clin. Pharm. Ther. 26 (2001) 331–342.

[17] T. Takagi, C. Ramachandran, M. Bermejo, S. Yamashita, L.X. Yu, G.L. Amidon, A provisional biopharmaceutical classification of the top 200 oral drug products in the United States, Great Britain, Spain, and Japan, Mol. Pharm. 3 (2006) 631–643.

[18] H.Z. Ogata, A. Ejima, Y. Kawatsu, Bioavailability of two preparations of furosemide and their pharmacological activity in normal volunteers. European journal of clinical pharmacology, Eur. J. Clin. Pharmacolo. 34 (1983) 791–796.

[19] M.A. Husain, S.U. Rehman, H.M. Ishqi, T. Sarwar, M. Tabish, Spectroscopic and molecular docking evidence of aspirin and diflunisal binding to DNA: a comparative study, RSC Adv. 5 (2015) 64335–64345.

[20] S.C.J.M. Cavalcante, S.M. Egwaga, R. Gie, P. Gondrie, A.D.H.P. Harries, B. Kumar, K.L.-v. Weezenbeck, S. Mase, R.M. Menzies, M. Nasehi, A. Nunn, M. Pai, H.U. Sch€unemann, A. Vernon, R.G. Vianzon, V. Williams, Treatment of Tuberculosis: Guidelines, 4th ed. World Health Organization, Geneva, 2010.

[21] J.R. Wang, C.J. Ye, B.Q. Zhu, C. Zhou, X.F. Mei, Pharmaceutical cocrystals of the anti-tuberculosis drug pyrazinamide with dicarboxylic and tricarboxylic acids, CrystEngComm 17 (2015) 747–752.

[22] R.G. Hall, R.D. Leff, T. Gumbo, Treatment of active pulmonary tuberculosis in adults: current standards and recent advances. Insights from the Society of Infectious Diseases Pharmacists, Pharmacotherapy 29 (2009) 1468–1481.

[23] L.Y. Wang, B. Tan, H.L. Zhang, Z.W. Deng, Pharmaceutical cocrystals of diflunisal with nicotinamide or isonicotinamide, Org. Process. Res. Dev. 17 (2013) 1413–1418.

[24] A.O. Surov, A.P. Voronin, A.N. Manin, N.G. Manin, L.G. Kuzmina, A.V. Churakov, G.L. Perlovich, Pharmaceutical cocrystals of diflunisal and diclofenac with theophylline, Mol. Pharm. 11 (2014) 3707–3715.

[25] A.O.L. Évora, R.A.E. Castro, T.M.R. Maria, M.T.S. Rosado, M.R. Silva, A.M. Beja, J. Canotilho, M.E.S. Eusebio, Pyrazinamide-diflunisal: a new dual-drug co-crystal, Cryst. Growth Des. 11 (2011) 4780–4788.

[26] J.S. Al-Otaibi, Y.S. Mary, Y.S. Mary, C.Y. Panicker, R. Thomas, Cocrystals of pyrazinamide with p-toluenesulfonic and ferulic acids: DFT investigations and molecular docking studies, J. Mol. Struct. 1175 (2019) 916–926.

[27] Q.Q. Wang, J. Xue, Z. Hong, Y. Du, Pharmaceutical cocrystal formation of pyrazinamide with 3-hydroxybenzoic acid: a terahertz and raman vibrational spectroscopies study, Molecules 24 (2019) 252–261.

[28] A. Rahman, Dendrimer based terahertz time-domain spectroscopy and applications in molecular characterization, J. Mol. Struct. 1006 (2011) 59–65.

[29] E.J. Slingerland, E.G.E. Jahngen, T.M. Goyette, R.H. Giles, W.E. Nixon, Terahertz absorption spectra of nitromethane, J. Quant. Spectrosc. Ra. 112 (2011) 2323–2329.

[30] J.B. Baxter, G.W. Guglietta, Terahertz spectroscopy, Anal. Chem. 83 (2011) 4342–4368.

[31] T.W. Crowe, T. Globus, D.L. Woolard, J.L. Hesler, Terahertz sources and detectors and their application to biological sensing, Philos Trans A Math Phys Eng Sci 362 (2004) 365–374.

[32] C.J. Strachan, T. Rades, K.C. Gordon, J. Rantanen, Raman spectroscopy for quantitative analysis of pharmaceutical solids, J. Pharm. Pharmacol. 59 (2007) 179–192.

[33] J. Xue, Y. Jiang, W. Li, L. Yang, Y. Xu, G. Zhao, G. Zhang, X. Bu, K. Liu, J. Chen, J. Wu, Structures and spectroscopic characterization of calcium chloride-nicotinamide, -isonicotinamide, -picolinamide and praseodymium bromide-nicotinamide complexes, Spectrochim. Acta A 137 (2015) 864–870.

[34] Y. Du, Q. Cai, J.D. Xue, Q. Zhang, Raman and terahertz spectroscopic investigation of cocrystal formation involving antibiotic nitrofurantoin drug and coformer 4-aminobenzoic acid, Crystals 6 (2016) 259–268.

[35] Y. Cheballah, A. Ziane, S. Bouarab, A. Vega, Density functional study of the optical response of FeN and CoN nitrides with zinc-blend and rock-salt structures, J. Phys. Chem. Solids 100 (2017) 148–153.

[36] M. Naseri, M.M. Abutalib, M. Alkhambashi, K. Salehi, A. Farouk, Density functional theory based prediction of a new two-dimensional TeSe2 semiconductor: a case study on the electronic properties, Chem. Phys. Lett. 707 (2018) 160–164.

[37] Q. Wu, M. Litz, X.C. Zhang, Broadband detection capability of Znte electro-optic field detectors, Appl. Phys. Lett. 68 (1996) 2924–2926.

[38] A. Rice, Y. Jin, X.F. Ma, X.C. Zhang, D. Bliss, J. Larkin, M. Alexander, Teraherz optical rectification from <110>zinc-blende crystals, Appl. Phys. Lett. 64 (1994) 1324–1326.

[39] M.J. Frisch, G.W. Trucks, H.B. Schlegel, G.E. Scuseria, M.A. Robb, J.R. Cheeseman, J.A. Montgomery, T. Vreven, K.N. Kudin, J.C. Burant, J.M. Millam, S.S. Iyengar, J. Tomasi, V. Barone, B. Mennucci, M. Cossi, G. Scalmani, N. Rega, G.A. Petersson, H. Nakatsuji, M. Hada, M. Ehara, K. Toyota, R. Fukuda, J. Hasegawa, M. Ishida, T. Nakajima, Y. Honda, O. Kitao, H. Nakai, M. Klene, X. Li, J.E. Knox, H.P. Hratchian, J.B. Cross, V. Bakken, C. Adamo, J. Jaramillo, R. Gomperts, R.E. Stratmann, O. Yazyev, A.J. Austin, R. Cammi, C. Pomelli, J.W. Ochterski, P.Y. Ayala, K. Morokuma, G.A. Voth, P. Salvador, J.J. Dannenberg, V.G. Zakrzewski, S. Dapprich, A.D. Daniels, M.C. Strain, O. Farkas, D.K. Malick, A.D. Rabuck, K. Raghavachari, J.B. Foresman, J.V. Ortiz, Q. Cui, A.G. Baboul, S. Clifford, J. Cioslowski, B.B. Stefanov, G. Liu, A. Liashenko, P. Piskorz, I. Komaromi, R.L. Martin, D.J. Fox, T. Keith, M.A. Al-Laham, C.Y. Peng, A. Nanayakkara, M. Challacombe, P.M.W. Gill, Gaussian 03, Revision E. 01, Gaussian, Inc, Wallingford, CT, 2004.

[40] S. Shahab, H.A. Almodarresiyeh, L. Filippovich, F.H. Hajikolaee, R. Kumar, M. Darroudi, M. Mashayekhi, Geometry optimization and excited state properties of the new symmetric (E)-Stilbene derivative for application in thermostable polarizing PVA-films: a combined experimental and DFT approach, J. Mol. Struct. 1119 (2016) 423–430.

[41] P.F. Taday, I.V. Bradley, D.D. Arnone, M. Pepper, Using terahertz pulse spectroscopy to study the crystalline structure of a drug: a case study of the polymorphs of ranitidine hydrochloride, J. Pharm. Sci. 94 (2003) 831–838.

[42] Q. Cai, J.D. Xue, Q.Q. Wang, Y. Du, Investigation into structure and dehydration dynamic of gallic acid monohydrate: a raman spectroscopic study, Spectrochim. Acta A 201 (2018) 128–133.

[43] Q. Cai, J. Xue, Q. Wang, Y. Du, Solid-state cocrystal formation between acyclovir and fumaric acid: terahertz and raman vibrational spectroscopic studies, Spectrochim. Acta A 186 (2017) 29–36.

[44] P.M. Hakey, M.R. Hudson, D.G. Allis, W. Ouellette, T.M. Korter, Examination of phencyclidine hydrochloride via cryogenic terahertz spectroscopy, solid-state density functional theory, and X-ray diffraction, J. Phys. Chem. A 113 (2009) 13013–13022.

[45] Y. Du, Q. Cai, J. Xue, Q. Zhang, D. Qin, Structural investigation of the cocrystal formed between 5-fluorocytosine and fumaric acid based on vibrational spectroscopic technique, Spectrochim. Acta A 178 (2017) 251–257.

[46] A.R. Pallipurath, F. Civati, J. Sibik, C. Crowley, J.A. Zeitler, P. McArdle, A. Erxleben, A comprehensive spectroscopic study of the polymorphs of diflunisal and their phase transformations, Int. J. Pharm. 528 (2017) 312–321.